Journal of Biomedical Optics

BiomedicalOptics.SPIEDigitalLibrary.org

Multiphoton fluorescence lifetime imaging microscopy reveals free-to-bound NADH ratio changes associated with metabolic inhibition

Krystyna Drozdowicz-Tomsia
Ayad G. Anwer
Michael A. Cahill
Kaiser N. Madlum
Amel M. Maki
Mark S. Baker
Ewa M. Goldys

SPIE.

Journal of Biomedical Optics 19(8), 086016 (August 2014)

Multiphoton fluorescence lifetime imaging microscopy reveals free-to-bound NADH ratio changes associated with metabolic inhibition

Krystyna Drozdowicz-Tomsia,[a,*] Ayad G. Anwer,[a] Michael A. Cahill,[b] Kaiser N. Madlum,[c] Amel M. Maki,[c] Mark S. Baker,[d] and Ewa M. Goldys[a,e]

[a]Macquarie University, MQ BioFocus Research Centre/Department of Physics and Astronomy, North Ryde, New South Wales, 2109 Australia
[b]Charles Sturt University, School of Biomedical Sciences, Wagga Wagga, New South Wales, 2678 Australia
[c]University of Baghdad, Institute of Laser for Postgraduate Studies, Baghdad 10071, Iraq
[d]Macquarie University, Department of Chemistry & Biomolecular Sciences, North Ryde, New South Wales, 2109 Australia
[e]Macquarie University, ARC Centre of Excellence in Nanoscale Biophotonics, North Ryde, New South Wales, 2109 Australia

Abstract. Measurement of endogenous free and bound NAD(P)H relative concentrations in living cells is a useful method for monitoring aspects of cellular metabolism, because the NADH/NAD^+ reduction-oxidation pair is crucial for electron transfer through the mitochondrial electron transport chain. Variations of free and bound NAD(P)H ratio are also implicated in cellular bioenergetic and biosynthetic metabolic changes accompanying cancer. This study uses two-photon fluorescence lifetime imaging microscopy (FLIM) to investigate metabolic changes in MCF10A premalignant breast cancer cells treated with a range of glycolysis inhibitors: namely, 2 deoxy-D-glucose, oxythiamine, lonidamine, and 4-(chloromethyl) benzoyl chloride, as well as the mitochondrial membrane uncoupling agent carbonyl cyanide m-chlorophenylhydrazone. Through systematic analysis of FLIM data from control and treated cancer cells, we observed that all glycolytic inhibitors apart from lonidamine had a slightly decreased metabolic rate and that the presence of serum in the culture medium generally marginally protected cells from the effect of inhibitors. Direct production of glycolytic L-lactate was also measured in both treated and control cells. The combination of these two techniques gave valuable insights into cell metabolism and indicated that FLIM was more sensitive than traditional biochemical methods, as it directly measured metabolic changes within cells as compared to quantification of lactate secreted by metabolically active cells. [DOI: 10.1117/1.JBO.19.8.086016]

Keywords: optics; photonics; light; lasers; fluorescence; fluorescence lifetime imaging.

Paper 140221R received Apr. 7, 2014; revised manuscript received Jun. 17, 2014; accepted for publication Jul. 2, 2014; published online Aug. 20, 2014.

1 Introduction

The oxidized and reduced redox cofactor pairs flavin adenine dinucleotide ($FAD/FADH_2$) and nicotinamide adenine dinucleotide (NAD^+/NADH) are becoming increasingly recognized as key metabolic indicators of the state of cellular metabolism associated with health and disease. During the glycolytic conversion of glucose to pyruvate, NAD^+ is converted to NADH, and two acidic pyruvate molecules are created from each glucose. This threatens to deplete the cytoplasm of NAD^+ and to lower its pH. If the pyruvate carbon skeleton is not transferred to the mitochondria with consumption of NADH and fully oxidized to CO_2, mammalian cells must reduce pyruvate to lactate via lactate dehydrogenase to regenerate NAD^+. Lactate is then secreted via specific monocarboxylate transporters to maintain cellular pH.[1] Such biology is exhibited by cells under hypoxic conditions and is also typical of many cancer cells, which exhibit increased glycolytic biology even in the presence of oxygen (which is called aerobic glycolysis). Such a shift from oxidative phosphorylation to glycolysis for ATP production (the so-called Warburg effect) is one of the hallmarks of carcinogenesis.[2–6] Acidification of cellular environments can lead to cellular toxicity;[7,8] therefore, cells with predominantly glycolytic metabolism influence the state of health of other cells in the surrounding tissue. It remains to be measured how significant such subtle changes might be in a tumor environment, which will require extremely precise measurement of potentially slight metabolic change.

This emphasizes the great level of attention that has been directed toward potential therapeutic interventions based upon cancer-specific metabolism.[2–6] Perturbations in NAD^+/NADH are also associated with other pathologies, including diabetes, neurodegenerative diseases, inflammation,[9–11] and the very process of mammalian aging.[12] A decline in nuclear NAD^+ levels is associated with progeriatric defective mitochondrial biogenesis, which leads to subsequent increased oxidative damage and mutagenesis. Strikingly, this effect could be rectified by supplying the NAD^+/NADH precursor nicotinamide mononucleotide to cultured cells or to mice, giving aged cells a young phenotype.[12] Therefore, rapid, noninvasive methods to measure and manipulate cellular metabolic states and NAD^+/NADH levels, in particular, are highly desirable and relevant to the investigation of a variety of biomedical research areas.

Although NADH and NADPH are distributed throughout the cytosol, in cells with an active tricarboxylic acid cycle (TCA), >60% of intracellular NADH is typically localized in mitochondria, where it participates in oxidative phosphorylation

*Address all correspondence to: Krystyna Drozdowicz-Tomsia, E-mail: krystyna.drozdowicz-tomsia@mq.edu.au

and TCA, while the remainder is found in the cytoplasm (where it takes part in glycolysis) and the nucleus (where it is involved in transcriptional pathways). NADH autofluorescence is sensitive to modulation of metabolism, such as hypoxia, serum starvation, cell confluence, and mitochondrial uncoupling agents, such as potassium cyanide). The concentration of NADH is also sensitive to the onset of mitochondrially mediated apoptosis and the dissipation of membrane potential often caused by the uncoupler agents.[9,13,14]

A number of microscopic methods are available to measure the fluorescence of endogenous metabolites, including the coenzymes NADH and FAD. The spectral properties of NADH and NADPH are too similar to be discriminated by fluorescence microscopy and, thus, these two are often jointly referred to as NAD(P)H. NAD(P)H and FAD exhibit fluorescence maxima of 450 and 535 nm, respectively, when excited by single photons around 340 nm [NAD(P)H] and around 450 nm (FAD). Relative intensities of these two fluorescent signals can be used to estimate a redox ratio model of cellular metabolic status.[13] The levels of NAD(P)H and FAD can be reliably determined in living cells and tissues.[9,13,15] With the implementation of multiphoton microscopy, these fluorophores can be excited using two lower-energy photons within the 710- to 780-nm range for NAD(P)H and 700 to 900 nm for FAD, respectively. Two-photon excitation is preferred rather than single-photon excitation as it avoids UV light–induced cell damage. Also, the penetration into tissue is much deeper and the autofluorescence background is greatly reduced, leading to improved signal-to-noise ratio.[16,17]

Fluorescence lifetime imaging microscopy (FLIM) provides a functional noninvasive imaging technique that is able to detect differences in the lifetime of fluorescent signals. Fluorescence lifetime is a quantity that is independent of signal intensity; hence, fluorescence lifetime is unrelated to fluorophore concentration. Since it is a microscopic technique, it provides information about the lifetime of fluorophore molecules in the full spatial context of a cell. Moreover, FLIM is able to detect not just the presence of a fluorophore, but also some properties of its physical environment. This is important for NAD(P)H, which may exist in cells as a free molecule or be bound as a cofactor to enzymes. These free and enzyme-bound forms of NAD(P)H exhibit different fluorescence lifetimes of 0.4 to 0.5 ns for free NAD(P)H and 2 to 2.5 ns for the bound form of NAD(P)H, respectively.[18,19] The reason for this difference is that two NAD(P)H nucleotide rings of adenine and nicotinamide are thought to alternate in solution between an extended conformation and a folded one that permits interaction between resonant electrons from different nucleotides within one NAD(P)H molecule to enable emission of the fluorescent photon. Binding to the active site of an enzyme conformationally restricts the NAD(P)H molecule, and consequently, it prolongs its fluorescence lifetime.[17] It is important to note that the fluorescence decay of protein-bound NAD(P)H varies slightly for each of the multiple binding partners. Also, this binding leads to a multiexponential decay profile, with some decay constants comparable to those for free NAD(P)H.[20] Usually this decay is modeled using two components with few other approaches. In cerebral tissue, Yaseen et al.[21] fitted their data using four different components (C1 to C4) for the NAD(P)H decay fluorescence. Component C1 exhibited the shortest lifetime of ~0.4 ns and C2 showed a lifetime of ~1 ns, which were assigned to the different folding conformations of free NADH. C3 exhibited a lifetime of ~1.7 ns, which was associated with the lifetime observed for NADH bound to malate dehydrogenase or lactate dehydrogenase. C4 exhibited a peak lifetime of 3.2 ns, which was interpreted as possibly representing the NADH bound to large mitochondrial enzyme and which, therefore, could potentially serve as a useful indicator of changes in oxidative metabolism. In metabolically active cells, more of the NAD(P)H pool is enzyme bound, enabling FLIM to provide insights into real-time variations of metabolic activity in living cells since both the fluorescence lifetime and the ratio of free:bound NAD(P)H are greater in actively proliferating cells.[9,17,18,22] In general, cancer cells exhibit an elevated level of free NAD(P)H compared to normal nontransformed cells of similar origin. This is confirmed by time-resolved fluorescence studies of metastatic and nonmetastatic murine melanoma cell lines, as well as human tumorigenic lung cancer, bronchiolar epithelial, and breast cancer cells, which show that the average lifetime of NAD(P)H is lower in a variety of metastatic cells than in nonmetastatic cells. Specifically, nonmalignant cells exhibit mean lifetimes in the range of 1.4 to 1.9 ns, whereas malignant cell lifetimes are in the range of 0.5 to 0.85 ns.[23]

In this study, we assess the sensitivity of the FLIM method to detect minor metabolic variations on the level of individual cells. To this aim, we selected a precancerous breast cancer cell line MCF10A, where the glycolytic character of metabolism is not yet well pronounced. As the FLIM technique has been shown to detect variations between significantly different metabolic activities in malignant and nonmalignant cells, we tested whether it could detect much more subtle effects of metabolic inhibitors. We attempted to intervene into the metabolism of these cells and induce subtle metabolic changes by using the following inhibitors of metabolic pathways: 2-deoxy-D-glucose (2-DG), oxythiamine (OT), lonidamine (LND), and 4-(chloromethyl) benzoylchloride (4-CMBC).

2-DG is a synthetic glucose analogue, which should potentially affect many glucose-dependent reactions, but has been historically considered as an inhibitor of glycolysis. It is transported into cells via membrane glucose transporters and then phosphorylated to 2-DG-P by a hexokinase (HK), which is the first and rate-limiting reaction in glycolysis. However, lacking a 2-hydroxyl group, it cannot be metabolized by phosphogluco isomerase, the next glycolytic enzyme. Thus, 2-DG-P accumulates in the cytoplasm, where it competitively inhibits HK, reducing the entry of glucose to the glycolytic pathway and lowering ATP levels.[24–26] 2-DG also exerts diverse pleiotropic effects independent of glycolytic inhibition, such as activation of phosphatidylinositol-3-kinase, Akt, and multiple downstream targets of that signal transduction pathway in a variety of cell lines.[27]

OT is an antivitamin derivative of thiamine, which, after phosphorylation, shows high affinity to thiamine-dependent enzymes and decreases their activity. OT is phosphorylated in the same way as thiamine by the enzyme thiamine pyrophosphokinase to create thiamine pyrophosphate (TPP), a cofactor for several enzymes, including pyruvate dehydrogenase and the key pentose phosphate pathway (PPP) enzyme transketolase (TK).[5,28–30] The PPP activity affects cell proliferation because it provides the ribose required for nucleic acid biosynthesis as well as produces NADPH, which provides the essential reducing power utilized in a plethora of biosynthetic reactions and redox regulation.[2] OT is also likely to exert other pleiotropic effects. A dramatic decrease in tumor cell proliferation after the

administration of OT has been observed in several *in vitro* and *in vivo* tumor models, which has been interpreted as due to direct inhibition via TK of PPP reactions, which causes a G1 cell cycle arrest without interference with cell energy production.[30–32] However, a large variety of enzymes catalyzing many different classes of reactions require the coenzyme TPP,[33–35] and because of that, OT is expected to exhibit cell-type-specific confounding pleiotropic effects.

LND was thought for several decades to be a specific inhibitor of mitochondrially bound HK and, therefore, to specifically inhibit glycolysis by lowering the number of glucose molecules that enter the glycolytic pathway, as well as to affect membrane integrity. More recent work has shown that LND is an inhibitor of a monocarboxylate transporter responsible for the secretion of lactate from the cytoplasm under conditions where mitochondrial TCA and oxidative phosphorylation did not eliminate the pyruvate formed by glycolysis (e.g., hypoxia, aerobic glycolysis). The resulting accumulation of cytoplasmic lactate results in cytoplasmic acidification, and this drop in pH was proposed to affect the activity of enzymes, such as HK, and the integrity of membranes.[1] Inhibition of monocarboxylate transport by LND was confirmed in 2013.[36]

4-CMBC is used as an early building block in the solid-phase synthesis of the tyrosine kinase inhibitor Imatinib (Gleevec).[37] It has been discussed in a 2010 paper as an experimental Wingless-Int (WNT) pathway inhibitor,[38] and data to that effect were published in a PhD thesis in 2011.[39] However, to our knowledge, no peer-reviewed source confirms that mechanism or any other although it is employed as an initiator of atom transfer radical polymerization in polymer chemistry.[40] 4-CMBC applied at 10 μM concentration was reported to decrease WNT signaling activity in VCaP prostate cancer cells.[38] WNT signaling plays a critical role in embryonic development and in adult tissue homeostasis. Inappropriate WNT signaling is closely linked to the occurrence of a number of malignant tumors, including breast and colon cancer.[41] WNT induces a glycolytic switch via increased glucose consumption and lactate production, with induction of pyruvate carboxylase.[42] Recent studies report that aerobic glycolysis (Warburg effect) could be induced by WNT 3A via increasing the level of key glycolytic enzymes.[43] Thus, although we are unaware of peer-reviewed literature verifying the mechanism of the action of 4-CMBC in mammalian cells, we considered the potential link to glucose metabolism to be worthy of study for its potential effects on NAD(P)H levels.

Carbonyl cyanide m-chlorophenyl hydrazone (CCCP) is a chemical inhibitor of oxidative phosphorylation. CCCP affects protein synthesis reactions in mitochondria, causing uncoupling of proton gradients that are established during normal activity of the electron transport chain. The chemical acts essentially as an ionophore and reduces the ability of ATP synthase to function optimally.[44]

In this work, we test the hypothesis that the inhibitors 2-DG, OT, LND, 4-CMBC, and CCCP can observably modify average lifetimes and free:bound NAD(P)H ratios in living cells. We also explore whether FLIM is able to detect minor inhibitor-induced changes within each individual cell, such as differentiation between mitochondrial, cytoplasmic, and nuclear subcompartments. We selected an extreme case of premalignant MCF10A cells for our study, where the expected differences should be even smaller than in more advanced cancer. This issue has not been investigated previously to our knowledge, but the changes in NAD(P)H fluorescent lifetimes and free:bound NAD(P)H ratios at different perturbations (confluence, serum starvation, potassium cyanide (KCN) treatment) were previously measured and reported for MCF10A cells.[22]

2 Materials and Methods

2.1 *Cell Lines and Culture*

MCF10A cells are an immortalized, nontransformed epithelial cell line derived from human fibrocystic mammary tissue. These cells are defined as precancerous breast cells; they have a near-diploid karyotype and are dependent on exogenous (serum) growth factors for proliferation.[45,46] MCF10A cells were obtained from the American Type Culture Collection and cultured as described.[45] Prior to inhibitor additions, MCF10A cells were plated onto cover glass bottomed Petri dishes 22 mm in diameter. All incubation processes for all cells were performed in an incubator type Forma Series II Water Jacketed CO_2 Incubator from Thermo Scientific (Waltham, Massachusetts), which was set to 37°C and with the injection of 5% CO_2 gas [food grade from The British Oxygen Company (BOC)]. All used chemicals, including buffers and solvents, were purchased from Sigma-Aldrich Pty Ltd. (Sydney, New South Wales, Australia) unless otherwise noted.

2.2 *Effect of CCCP on NAD(P)H Lifetime*

MCF10A cells were cultured on sterile coverslips of Petri dishes for three days before the treatment with CCCP (C2759 from Sigma-Aldrich). As a culture medium, we used mammary epithelial basal medium (MEBM) (Lonza, Basel, Switzerland) supplemented with 3% horse serum in the first experiment and serum free in the other. Cell suspension (100 μl) was added to the center of each dish and incubated at 37°C. After 24 h, 1 ml of fresh medium was added for each dish and cells were incubated for another two days. After that, CCCP (50 mM stock solution in dimethyl sulfoxide (DMSO)) was prepared: 10 μl was added to 10 ml of the medium to attain a final concentration of 50 μM. Then each dish in the treatment group received 1 ml of CCCP, with controls receiving only the medium. FLIM data were collected from each dish 5, 10, 15, 20, 25, 30, and 60 min after treatment. Data were collected at 60-s acquisition times at 740-nm excitation.

2.3 *Effect of Other Inhibitors on NAD(P)H Lifetime*

MCF10A cells were cultured on glass coverslips for two days before treatment as described for CCCP treatments above. Coverslips were placed in plastic tissue culture Petri dishes (seven coverslips in each Petri dish), and 100 μl of cell suspension was added to the center of each coverslip followed by incubation at 37°C for up to 48 h. After 1, 2, 24, and 48 h, three coverslips from the treated group (with one of the inhibitors below) and one from the control group were washed three times with Hank's balanced salt solution (HBSS, Invitrogen, Carlsbad, California) and mounted on concave slides containing ~50 μl HBSS. With such protocol, all treated and control samples were at the same confluences and were grown in the same serum-rich or under starvation conditions to detect differences only due to inhibitor treatment. FLIM data were collected for the slides of control and treated groups. The acquisition time for the cells was 90 s (more details in Sec. 2.6) to prevent cell damage or photobleaching. The inhibitors listed below were used.

2.3.1 *Lonidamine*

LND (L4900, Sigma-Aldrich) was dissolved in DMSO and mixed with MEBM medium to a final concentration of 20 μM. Four milliliter of the mixture was added to each Petri dish with the coverslips. The third Petri dish with control cells received 4 ml of the medium without LND and all were incubated.

2.3.2 *Oxythiamine*

A 100-mM stock solution of OT (O4000, Sigma-Aldrich) in DMSO was prepared: 2 μl was added to 8 ml MEBM medium to provide a final concentration of 25 μM. Then, 4 ml of the mixture was added to each Petri dish with the coverslips; the third Petri dish that contains the control cells received 4 ml of the medium without OT and all were incubated.

2.3.3 *4-(chloromethyl) benzoyl chloride inhibitor*

A 42.2-mM stock solution of 4-CMBC (270784, Sigma-Aldrich) was prepared in DMSO: 9.5 μl was added to 10 ml MEBM medium to obtain a final concentration of 40 μM. Then, 4 ml of the mixture was added to each Petri dish with the coverslips. The third Petri dish with control cells only received 4 ml of the medium without 4-CMBC and all were incubated.

2.3.4 *2-deoxy-D-glucose*

A 100-mM stock solution was prepared by dissolving 2-DG (D8375, Sigma-Aldrich) in distilled water: 3 μl was added to 12 ml MEBM medium to give a final concentration of 25 μM. Each coverslip was transferred to a separate Petri dish 22 mm in diameter and 1 ml of the mixture was added to 12 dishes. Four dishes were used as controls without addition of 2-DG and all were incubated.

2.4 *Mitochondrial Membrane Potential Experiment*

The cells were treated with 50 μM CCCP (C2759 from Sigma-Aldrich). After CCCP treatment of all dishes, the JC-1 stain (Life Technologies, Carlsbad, California) was used for labeling cells treated with CCCP and controls. A 200-μM of JC-1 stock solution was prepared by dissolving the contents of one vial in 230 μl of DMSO provided. Cells were incubated with JC-1 at a final concentration of 2 μM, followed by incubation for 20 min and washing in phosphate-buffered saline (PBS). Labeled cells were imaged using the Leica SP2 confocal microscope. For each group of control and treated cells, spectral images were collected at 488-nm excitation wavelength and detected in 10-nm windows in the 520- to 660-nm range. The collected data were unmixed to produce corrected spectra with peak emissions at 535 nm (green) and 590 nm (red), corresponding to monomeric and aggregated forms of JC-1, respectively. Unmixed images at these wavelengths were extracted and used to quantify the ratio between red and green fluorescence using the InCell Developer software (GE Healthcare, Albany, New York) to evaluate the mitochondrial membrane potential.

2.5 *Extracellular Lactate Assay*

A Cayman's Glycolysis Cell-Based Assay Kit (Abcam, United Kingdom) was used. This kit provides a colorimetric method for detecting extracellular L-lactate, the end product of non-oxidative glucose metabolism. Cells were cultured in a 96-well plate at a density of 10^4 to 10^5 cells/well in 120 μL of culture medium and incubated overnight. On the next day, cells in wells were treated with inhibitors for the same incubation times used for FLIM imaging. The kit standards and reaction solutions were prepared according to the kit protocol. From each well, 10 μl of cells supernatant was added to 90 μl of assay buffer in a new 96-well plate, followed by the addition of 100 μl of reaction solutions. A 96-well plate was then incubated with gentle shaking on an orbital shaker for 30 min at room temperature. The absorbance was measured at 490 nm using a Spectra MAX M5 Multi-Mode Microplate Reader (Molecular Devices, Sunnyvale, California). The concentrations of L-lactate were calculated from absorbance measurements, after collecting calibration curve using standards provided with the glycolysis kit.

2.6 *FLIM Imaging*

Multiphoton FLIM images were acquired on a Leica SP2 confocal microscope (Leica Microsystems, Wetzlar, Germany) equipped with Ti:sapphire mode-locking cavity laser (Spectra-Physics-Millennium-Tsunami, Santa Clara, California, 80 MHz, 100 ps) pumped by a frequency doubled YAG laser (532 nm) and the lifetime signal was detected using a fast photon counting detector (PMH-100, Becker & Hickl GmbH, Berlin, Germany). The excitation wavelength was set to 740 nm with average laser intensity of 7.8 mW and a narrow band-pass filter 452/45 nm was used to collect only the autofluorescence signal specific to NAD(P)H. Multiphoton FLIM images were acquired with an electronic system single photon counting module (SPCM) for recording fast light signals by time-correlated single-photon counting (SPC-830, Becker & Hickl GmbH). Synchronized fluorescence lifetime data collection on a pixel-by-pixel basis was achieved using the x and y laser scanning signals generated by the confocal scan unit with a pixel dwell time of 4.9 μs. FLIM data were collected through a 60× oil objective (NA = 1.3) with collection times ranging from 60 to 180 s during optimization to provide enough photons and prevent the cells' degradation. For all the measurements, 90 s was chosen as it produced sufficient intensity signal for data analysis, and a cell viability test showed that the cells were not affected. FLIM measurements were collected for healthy, viable, dividing cells at high confluences, but only from regions of cells forming a single layer and always at the same cross-section plane. This cross-section plane was established before each experimental day by test measurements of Fluoresbrite YG (10 micron) microspheres (from Polysciences, Warrington, Pennsylvania); this was also to test the accuracy and consistency of the FLIM system. The measured lifetime for these control beads was 2.19 ± 0.02 ns, in agreement with previous works.[15]

2.7 *Analysis of the Fluorescence Lifetime Decay Curves*

Time-decay FLIM data were fitted with a biexponential model using the vendor supplied software (SPCImage, v4.0.8.0, Becker & Hickl GmbH). First, the measured lifetime decay curve was binned over the pixel of interest and the eight nearest-neighbor pixels. Each set of binned pixels was fitted independently. The measured instrument response was mathematically removed from the measured data using deconvolution. This procedure yielded lifetime decay curves with peak values >100 counts. These lifetime decay curves for a given set of binned pixels were fitted to a double-exponential decay model.

$$F(t) = \alpha_1 \exp(-t/\tau_1) + \alpha_2 \exp(-t/\tau_2) + C,$$

where $F(t)$ is the fluorescence intensity at time t after the excitation light has ceased, τ_1 and τ_2 are the fluorophore lifetimes (τ_1 is the short-lifetime component and τ_2 is the long-lifetime component), α_1 and α_2 are the relative contributions of the lifetime components (i.e., $\alpha_1 + \alpha_2 = 100\%$), and C is an empirical constant related to the level of background light. The lifetime for the pixel of interest was calculated by finding the global minimum of the chi-squared χ^2 goodness of fit value. The minimum calculated lifetime constrained by the fitted model in SPCImage was 0.1 ns, which is close to the temporal response of the multiphoton FLIM system. A survey of the χ^2 values on a few samples indicated that the double-exponential decay model improved the fit compared to the alternative single-exponential and triple-exponential decay models. The measured sample decay trace and its fitting curve from a selected pixel is demonstrated in Fig. 1. From each lifetime image, the mean value and standard deviation of individual parameters, such as the biexponential lifetime components (τ_2, τ_1) and corresponding coefficients (α_1, α_2) for every pixel in the image were extracted. Only the pixels with a total intensity count >100 photons and with the mean and standard deviation of the χ^2 value of 1.05 ± 0.15, respectively, were used for further lifetime analysis for each image. Using these values, the weighted mean and standard deviation of each set of measurements were calculated to produce an average lifetime, short and long lifetimes corresponding to free and bound NAD(P)H, respectively, and their ratios. A student's t test was used to evaluate the observed differences between the sample means with a significance level of 0.05. FLIM data were collected for a minimum of three different spots on each slide and at least five replicate slides for each sample type and its controls were measured.

3 Results and Discussion

3.1 *Multiphoton FLIM Imaging and Effect of Inhibitors on NAD(P)H Lifetime*

Figure 1 shows an example of a multiphoton FLIM image of untreated MCF10A control cells and its analysis results for a binned pixel showing a good fit of the measured lifetime data to the biexponential model. The lifetime distribution in MCF10A cells shows the shortest NAD(P)H lifetimes in the nucleus and mitochondria and longer lifetimes for NAD(P)H in the cytosol, in agreement with previous observations from rodent cells.[15] Here we show that the same relationship is found for human MCF10A breast cells.

3.2 *Effect of 2-Deoxy-D-Glucose on NAD(P)H Fluorescence Lifetime*

FLIM images were collected from untreated MCF10A cells (controls) and treated with (25 μM) 2-DG in the presence and absence of serum. The extracted data are presented in Figs. 2(a) and 2(b) for different incubation times. Note that

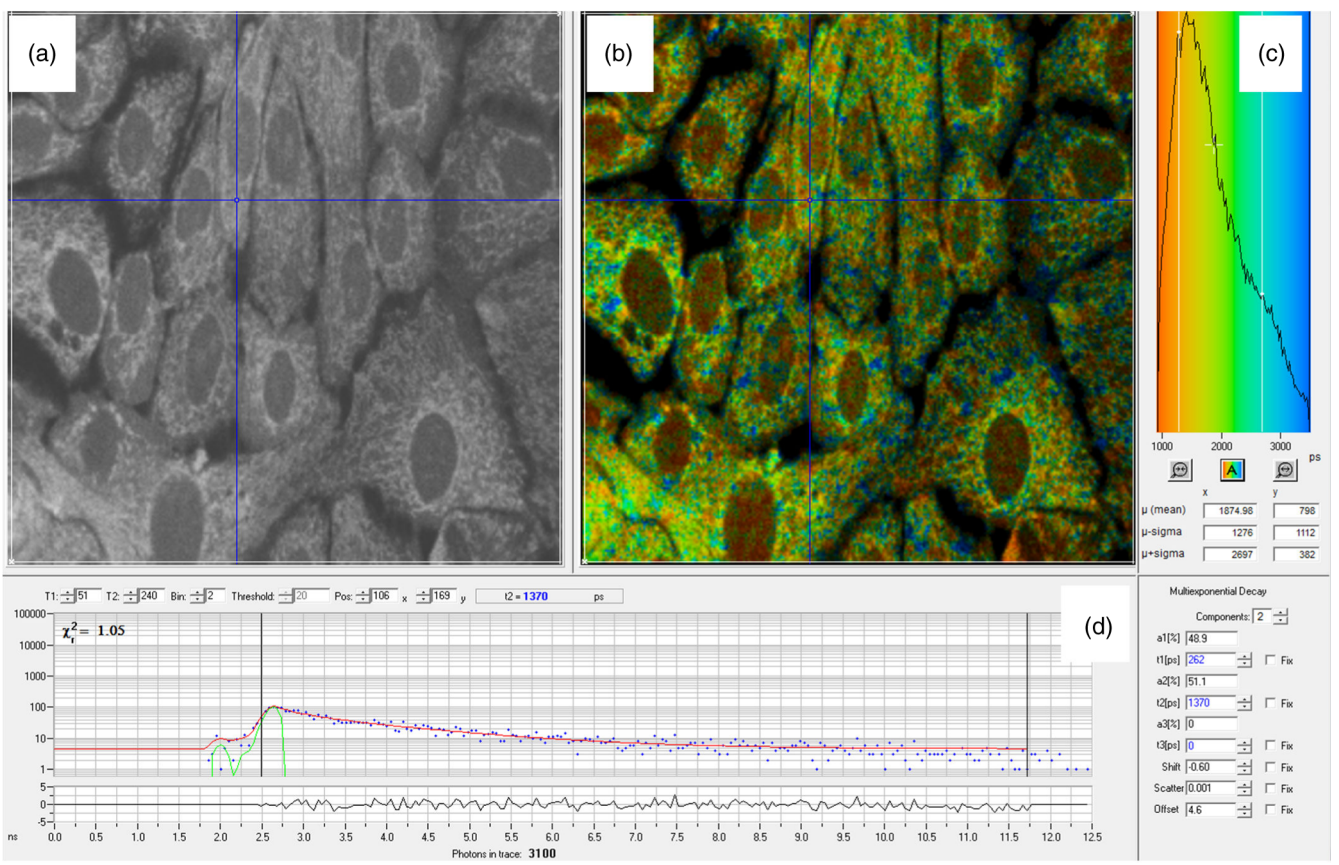

Fig. 1 Screenshot from SPCMImage software (Becker & Hickl Gmbh, Germany) of analyzed fluorescence lifetime imaging microscopy (FLIM) image of MCF10A cells untreated. (a) Intensity image. (b) Color-coded image of long lifetime component distribution. (c) Histogram of calculated long component τ_2 of lifetime for image (a). (d) Decay curve of multiexponential decay calculated with two component lifetime contributions, blue points—experimentally measured lifetimes, green curve—instrument response function, and red curve—calculated curve fit to experimental decay.

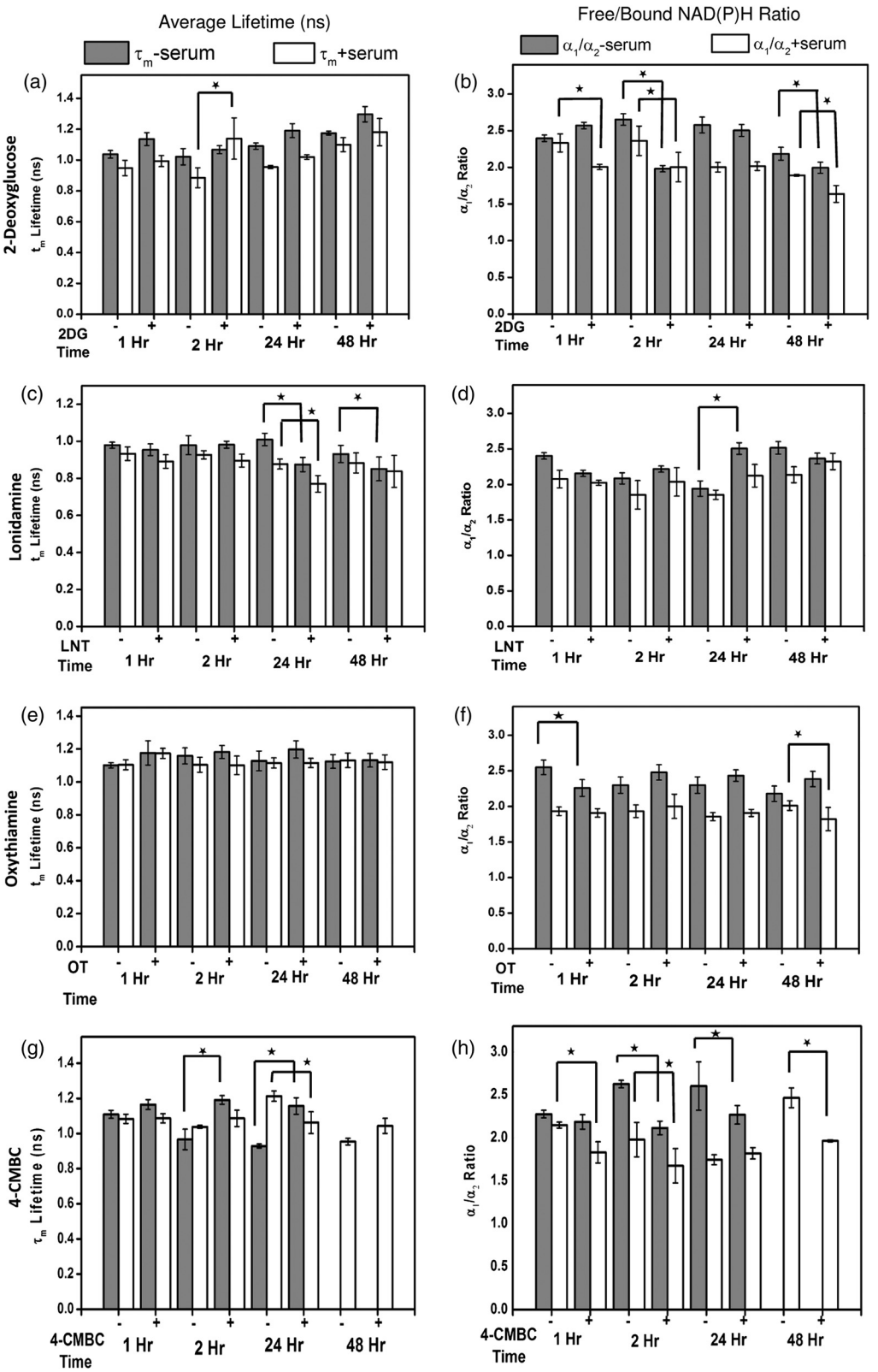

Fig. 2 Summary of lifetime measurements using FLIM for MCF10A cells grown with inhibitors measured at 1, 2, 24, and 48 h after adding the inhibitor and compared with their controls grown for the same period of time but without inhibitors in two medium types. Shaded columns correspond to MCF10A cells grown in medium without serum and white columns for cells grown with 3% serum and are shown for controls (–) and treated samples with inhibitors (+), respectively. Left column summarizes average lifetimes and right column shows free to bound NAD(P)H ratios for samples grown with following inhibitors: 2-deoxy-D-glucose (2DG) [(a) and (b)], lonidamine (LND) [(c) and (d)], oxythiamine (OT) [(e) and (f)], and 4-(chloromethyl) benzoylchloride (4-CMBC) [(g) and (h)]. Significant changes ($p < 0.05$) marked with stars were highlighted in the graphs.

our concentration of 2-DG is around three orders of magnitude lower than is commonly employed.[27,47] For all measured samples, lifetimes for free and bound NAD(P)H were in the following ranges: τ_1 in 0.36 to 0.52 ± 0.005 ns, τ_2 in 2.0 to 2.7 ± 0.05 ns, respectively, with free-to-bound NAD(P)H ratios in the range of 1.6 to 2.8 ± 0.05 and average lifetimes τ_m in 0.9 to 1.3 ± 0.05 ns range. After the inhibitor treatment, the average lifetimes were slightly longer than in the untreated samples. The samples without serum trended toward insignificantly higher average lifetimes and longer lifetimes for free and bound NAD(P)H than the samples with serum. In the medium supplemented with 3% serum, all treated cells also trended toward higher average lifetimes compared to controls. Statistically significant changes ($p > 0.05$) were observed only for a 2-h incubation period with the inhibitor for the sample grown in the medium with serum. This increase in average lifetimes was also accompanied by a significant decrease in free-to-bound NAD(P)H ratios for 2-DG-treated cells in serum observed for 1-, 2-, and 48-h incubation times. A significant decrease in the free:bound NAD(P)H ratio was observed in cells grown without serum and incubated with the inhibitor for 2 and 48 h.

We note that other authors also observed a decrease in the concentration of free NAD(P)H after treatment with 2-DG and a concomitant increase of the $NAD(P)^+/NAD(P)H$ ratio in the cytosol.[4,47–49] In our study, an extremely low concentration of 2-DG was used (25 μM) compared to previous works; however, significantly decreased levels of free:bound NAD(P)H ratios and increased average fluorescence lifetimes could be detected. Irrespective of the mechanism underlying these variations,[27] we show that FLIM microscopy provides quantitative data with sufficient precision to be an extremely sensitive method to detect subtle fluctuations in the metabolism of living cells. We are unaware of other studies having previously demonstrated this aspect of multiphoton FLIM microscopy.

We have been able to measure the changes in the relative contributions of free to protein-bound NAD(P)H before and after the treatment over the entire cellular volume, including its nuclear, cytosolic, and mitochondrial pools, where we observed a significant decrease after treatment for 1 and 2 h and a small decrease after 48 h in cells cultured with serum. However, the full picture is somewhat more nuanced. For example, the ratio of free:bound NAD(P)H (α_1/α_2) in the cytosol and the nucleus are slightly higher than that in the mitochondria.[14] 2-DG appears to affect the glycolysis in the cytosol, causing a significant decrease of the (α_1/α_2) ratio, reflecting a decrease of the ratio of free-overbound NAD(P)H. Because free NAD(P)H can diffuse through the nuclear pore, the change of free NAD(P)H in the nuclear compartment may be associated with the decrease of free NAD(P)H in the cytosol, or with its consumption there. NADH cannot simply pass into the mitochondria because the inner mitochondrial membrane is impermeable to NADH and NAD^+. Thus, the (α_1/α_2) ratio in the mitochondria is almost unchanged before and after our treatment, indicating that 2-DG may have little effect on the mitochondrial NADH equilibrium (data not shown here).

We also noticed a consistent difference in NAD(P)H florescence lifetimes of cells grown with and without serum for all experiments, also reported previously.[22] The addition of serum to the culture media is known to increase the growth rate of the cells by increasing the glucose metabolism in response to signaling.[50,51] Serum starvation dramatically increases the fraction of bound NAD(P)H in the nucleus.[52] The addition of a small amount of serum (2%) causes a decrease in the quantity of nuclear free NAD(P)H, which influences the overall colocalization of free and bound NAD(P)H within the nucleus, and an increase in free NAD(P)H within the cytoplasm. The cells exposed to 10% serum show a larger fraction of free NAD(P)H in the nucleus.[52] This effect of serum was also evident in our experiments in the control groups, where the (α_1/α_2) ratios were always lower in the presence of serum as compared to serum-free samples.

3.3 *Very Small Metabolic Changes Induced by LND Can be Detected Using NAD(P)H Fluorescence Lifetime*

We treated MCF10A cells with just 20 μM of LND in the presence and the absence of serum, at a lower concentration than that used in earlier works (45 to 600 μM).[1,36] The data extracted from FLIM images are presented in Figs. 2(c) and 2(d). For all measured samples, the lifetimes for free and bound NAD(P)H were in the following ranges: τ_1 in 0.38 to 0.49 ± 0.03 ns, τ_2 in 1.6 to 2.3 ± 0.05 ns, respectively, with free:bound NAD(P)H ratios in the range of 1.7 to 2.5 ± 0.03 and average lifetimes τ_m in 0.8 to 1.05 ± 0.05 ns range. The mean fluorescence lifetimes τ_m decreased after the treatment, contrary to the trends observed for the 2-DG treatment [see Fig. 2(c)]. A significant decrease ($p < 0.05$) was observed in the mean fluorescence lifetime after 24 h of treatment with LND in the presence and absence of serum. LND also significantly increased the ratio of free:bound NAD(P)H after 24 h for cells grown without serum. The same trend was observed for cells with serum, but it was not significant. These results are noteworthy since the change in intracellular pH induced by 80 μM LND inhibition of lactate transport was only marginal.[1] However, Figs. 2(c) and 2(d) detected clearly observable differences in both NAD(P)H lifetime and the ratio of free:bound NAD(P)H after 24 h.

3.4 *Effect of Oxythiamine on the NAD(P)H Fluorescence Lifetime*

FLIM images for MCF10A cells treated with 20 μM OT exhibited much less variability compared to samples treated with other inhibitors, as apparent in the lifetime data presented in Figs. 2(e) and 2(f). At this concentration, marked effects on cells (motility) have been observed.[35] For all measured samples, lifetimes for free and bound NAD(P)H were in the following ranges: τ_1 in 0.39 to 0.56 ± 0.005 ns, τ_2 in 2.25 to 2.65 ± 0.005 ns, respectively, with free:bound NAD(P)H ratios in the range of 1.8 to 2.5 ± 0.05 and average lifetimes τ_m in 1.1 to 1.2 ± 0.05 ns range. The mean fluorescence lifetime τ_m of NAD(P)H in MCF10A cells treated with OT in the presence or absence of serum are presented in Fig. 2(e). No significant differences were detected between control and treatment groups in the presence and in the absence of serum. The relative contributions of free and bound NAD(P)H [Fig. 2(f)] show only very small changes in the presence of serum, with a significant decrease ($p < 0.05$) only for samples treated for 48 h, and in absence of serum, the only significant difference was observed within the first hour of treatment.

In our study, there was no significant change in the mean fluorescence lifetime τ_m of NAD(P)H after the treatment with OT [Fig. 2(e)]. NADPH is produced by PPP and has the same fluorescence properties as NADH. Thus, alteration of NADPH

production by OT may have contributed to the difference in the experiment ratios of free:bound NAD(P)H. As the concentration of NADPH is about four to seven times lower than NADH in a range of tissue types,[53] the effect of metabolic perturbations on NAD(P)H fluorescence should be lower by a similar factor. Taken together, this suggests that the decrease in free NAD(P)H observed after 1 and 48 h of OT treatment [Fig. 2(f)] was caused by the inhibitory effect of OT. However, we cannot exclude the possibility that other metabolic pathways contributed to the result.

3.5 *Effect of 4-(Chloromethyl) Benzoyl Chloride on the NAD(P)H Fluorescence Lifetime*

The lifetime data extracted from FLIM images of MCF10A cells treated with 40 μM 4-CMBC in the presence or absence of 3% serum are presented in Figs. 2(g) and 2(h). For all measured samples, the lifetimes for free and bound NAD(P)H were in the following ranges: τ_1 in 0.44 to 0.56 $\pm$ 0.005 ns, τ_2 in 2.0 to 2.5 $\pm$ 0.05 ns, respectively, with free:bound NAD(P)H ratios in the range of 1.6 to 2.6 $\pm$ 0.05 and average lifetimes τ_m in 0.90 to 1.20 $\pm$ 0.005 ns range. Significant increases in the average lifetime of NAD(P)H fluorescence were observed at 2 and 24 h in the absence of serum, which were associated with cell death by 48 h, whereas a significant decrease in fluorescence lifetime was observed in the presence of serum at 24 h.

Figure 2(h) depicts the relative contributions of free and bound NAD(P)H after the treatment with 4-CMBC. A significant decrease ($p < 0.05$) in the α_1/α_2 ratio was observed in the presence of serum after 1, 2, and 48 h of treatment, while the 24-h sample showed a small increase compared to its control, well correlating with the changes in an average lifetime.

Regardless of its mechanism of action, in our experiment, 4-CMBC caused a slightly higher change in the mean fluorescence lifetime of NAD(P)H in the absence of serum and the changes were correlated with changes in free:bound NAD(P)H ratios between treated and control samples. This result may be attributed to a significant decrease in the viability of MCF10A cells grown in medium without serum treated with 4-CMBC, as the cell count was reduced to ~78% compared to controls after 24 h and <10% after 48 h (in the latter case, cells were not suitable for imaging). Cell viability was not altered in the presence of serum, indicating some protective activity against the inhibitor.

3.6 *Overview of the Effect of Investigated Inhibitors on Contribution of Free NAD(P)H*

In order to obtain an improved overview of the changes in the previously presented data, we calculated the relative percentage difference between the contribution of free NAD(P)H measured for MCF10A cells treated with different inhibitors and their respective nontreated controls for cells grown in the two types of medium. They are shown in Fig. 3 for samples grown without serum [Fig. 3(a)] and with 3% of serum [Fig. 3(b)]. The differences in contribution of free NAD(P)H for all cells treated with different inhibitors are within $\pm$30%. In the absence of serum, the variability is higher than for samples treated in the presence of 3% serum, and the highest reduction in free NAD(P)H was observed for treatment with 2-DG and 4-CMBC for 2 h, at 25 and 19%, respectively. OT exhibited the least effect for MCF10A treated cells with or without serum. In contrast, LND induced the highest increase in free NAD(P)H

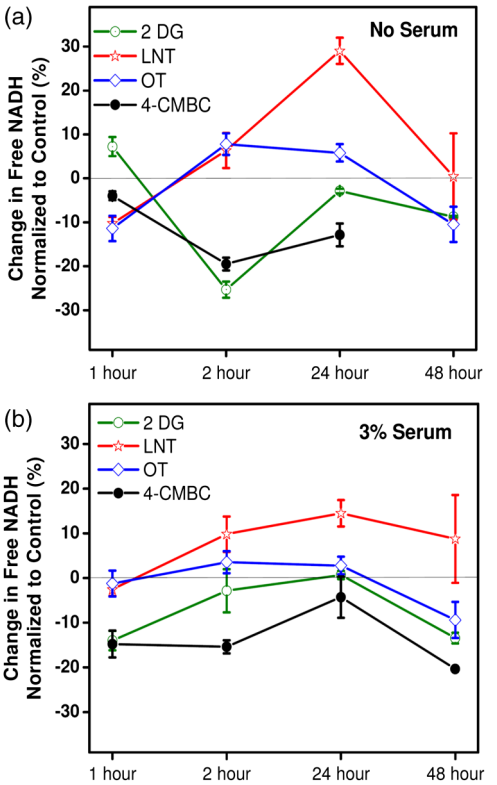

Fig. 3 Percentage difference in contribution of short component of lifetime, assigned to free NAD(P)H as compared to respective control and normalized to that control, for MCF10A cells treated with different inhibitors and measured for samples and controls incubated for 1, 2, 24, and 48 h from inhibitor treatment. Control samples were MCF10A cells cultured for the same times but without inhibitors. The experiments were conducted with medium without serum—graph (a) and with 3% serum—graph (b) and following inhibitors: 2DG, LND, OT, and 4-CMBC (see legend in the graphs).

contribution after 24 h treatment for samples without and with serum, 29 and 15%, respectively.

For samples with 3% serum, the changes in free NAD(P)H were less pronounced. For all treated samples, a reduction in free NAD(P)H was observed in the first hour for all inhibitors, after which cells showed some recovery for the next 2- and 24-h periods, followed by a decrease for samples treated for 48 h. Based upon our results, the strongest inhibition of free NAD(P)H (which can be associated with decreased metabolic activity) was observed for inhibitors in the following order: 4-CMBC > 2-DG > OT, and LND exhibited the apparent opposite effect. These LND-induced changes in the contribution of free NAD(P)H presumably involve changes in intracellular pH. LND is a well-established inhibitor of monocarboxylate transport,[1,36] so that lactate secretion should be impaired by LND, leading to cytoplasmic accumulation of lactate, which should decrease the cytoplasmic pH. We propose the following rationalization for our observed results. Mild LND-induced cytoplasmic acidification should induce a stress response and accompanying activation of glycolysis to produce pyruvate and, subsequently, lactate. Since the 20 μM concentration of LND employed was lower than the 50 μM required to achieve 50% inhibition of lactate secretion,[54] lactate should still have accumulated in the extracellular medium, which would have diminished the magnitude of any cytoplasmic pH change

attributable to LND inhibition of lactate transport. However, alternative mechanisms could not be ruled out.

3.7 *Effects of Inhibitors on Lactate Secretion*

Figure 4 shows results of lactate secretion measurements for MCF10 cells grown in medium with 3% serum, and Fig. 5 presents results of the same experiment for cells without serum, treated with four inhibitors at 1, 2, 24, and 48 h. Here, we measured the level of L-lactate concentration in the supernatant of treated cells. These results show that for cells grown in medium with serum only, the treatment with 2-DG led to a noticeable decrease in lactate secretion at 1 and 2 h. For other inhibitors, the changes in the level of L-lactate upon inhibitor treatments were insignificant. A small decrease of concentration was observed at 1- and 48-h treatments with OT and in the first hour for 4-CMBC. LND-treated MCF10A cells grown in medium with serum showed a slight increase in the level of lactate after 1 and 2 h after the inhibitor treatment and a slight decrease for the 24-h sample. In the case of 4-CMBC, a small increase was observed only for the 2 h of treatment, but for other periods, no differences were detected.

In cells placed in a medium without serum, slightly higher variations between control and treated cells were observed and are shown in Fig. 5. The treatment with 2-DG inhibitor led to a noticeable decrease in secreted lactate for 1 and 2 h after treatment. An increase in lactate concentration in cells treated with LND and with OT was observed after 2 h of treatment. For cells treated with 4-CMBC, no differences were observed with respect to controls, and only a small decrease for the 24-h treatment.

In all lactate secretion experiments performed using the Cayman glycolysis kit, the concentration levels of lactate are measured after secretion to the media. Levels were in the 0.1- to 1-μM range after 1 and 2 h of inhibitor treatment and in 1- to 10-μM range for 24 and 48 h. This difference in measured concentrations over time is related to increased number of secreting cells. These experiments detected very little change in lactate secretion as a result of the application of the inhibitors. The small differences observed here for different inhibitors are consistent with the results of FLIM analysis and with the low levels of inhibitors employed here. We confirmed that the secretion of L-lactate was most affected by 2-DG (which caused a decrease in lactate concentration) and LND (which caused

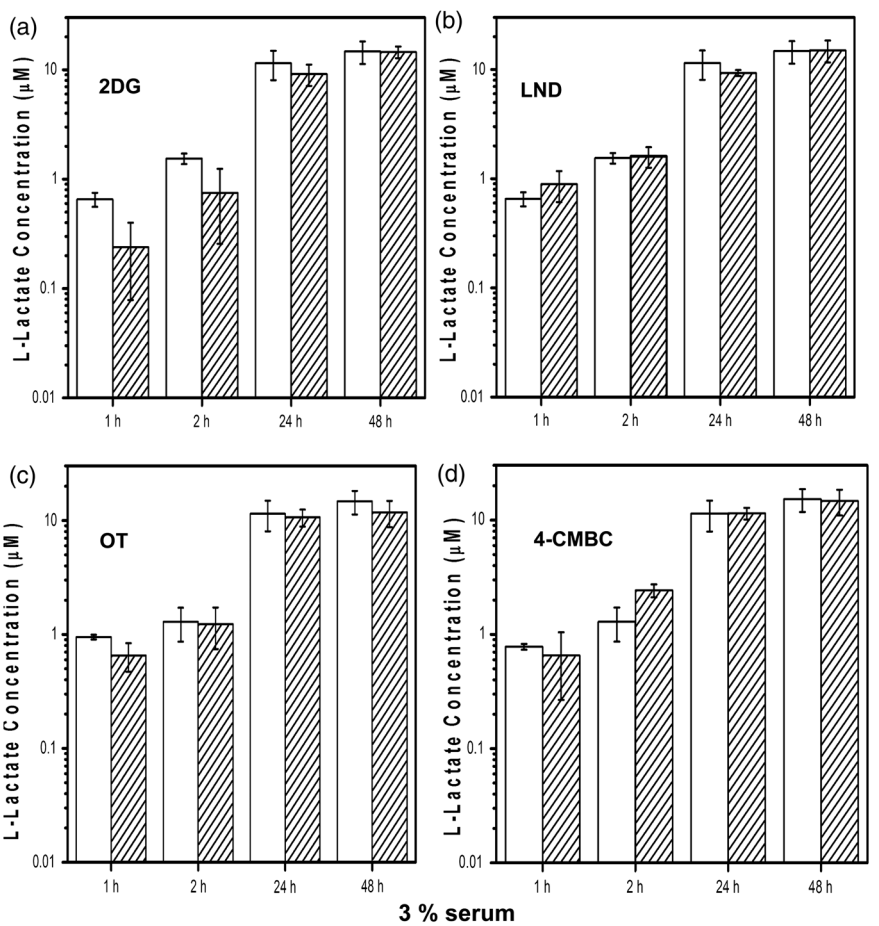

Fig. 4 Results of lactate production for MCF10 cells grown in medium with 3% serum, treated with various inhibitors: (a) 2DG, (b) LND, (c) OT, (d) 4-CMBC, and measured at intervals of 1, 2, 24, and 48 h from inhibitor treatment. Bars correspond to control samples—shown in white, treated samples—shown as dashed bars. L-lactate concentration in supernatant taken from controls and treated samples was measured by absorbance measurements and compared to calibration curve obtained using standards from the Cayman glycolysis kit.

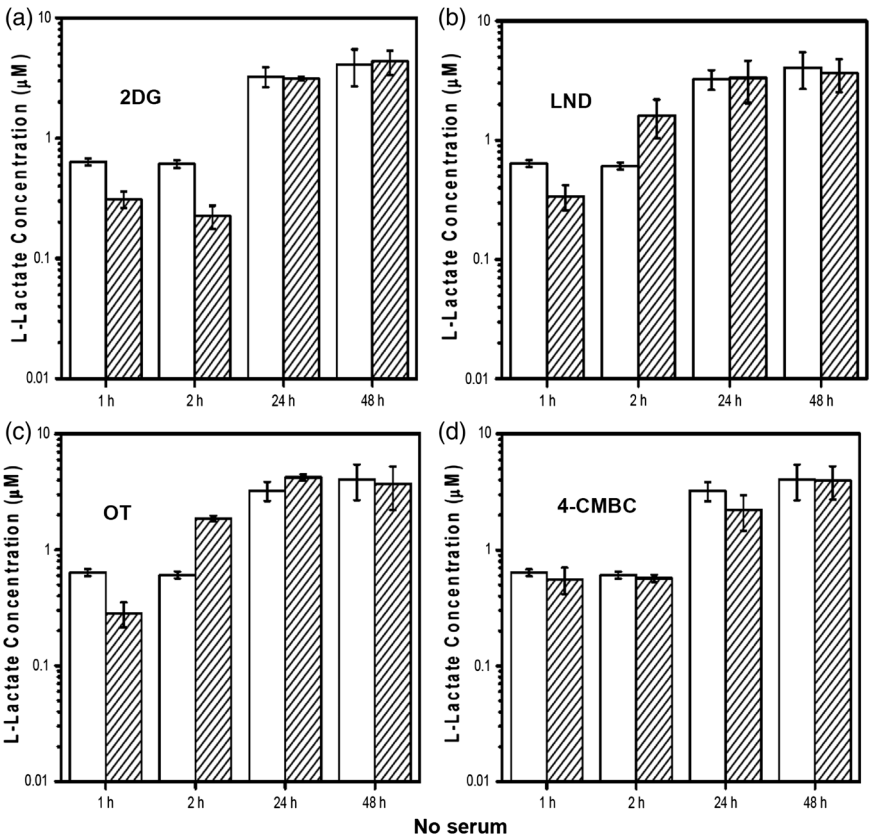

Fig. 5 Results of glycolysis measurements for MCF10 cells grown in medium without serum, treated with various inhibitors: (a) 2DG, (b) LD, (c) OT, and (d) 4-CMBC, and measured at intervals of 1, 2, 24, and 48 h from inhibitor treatment. All data are plotted using the same conventions as in Fig. 4.

an increase). These results are consistent with our hypothesis that the low LND concentration used here partially inhibits lactate transport, inducing mild cytoplasmic acidification, which in turn hypothetically increases glycolytic activity. The poorest consistency between FLIM and measured lactate secretion levels was observed for the 4-CMBC inhibitor, as this inhibitor caused a significant decrease in cell viability. In that respect, in FLIM measurements, the data were collected from regions of similar cell density for treated and untreated cells and should accurately correspond to internal free:bound NAD(P)H ratio differences. However, the lactate secretion experiment measures bulk cell population properties as it indirectly quantifies bulk lactate secreted to the surrounding medium by all cells in the culture. Decreased cell viability upon treatment made comparisons at the later time points impossible to complete.

3.8 *Effect of Mitochondria Membrane Potential Inhibition on NAD(P)H Lifetime*

Figures 6(a) and 6(b) show the results of NAD(P)H fluorescence lifetime for cells incubated with and without serum and treated with CCCP for different times. It shows that the ratio of free: bound NAD(P)H decreases in cells treated with CCCP and incubated with or without serum, with larger fluctuations in the absence of serum. There is also more variation in the NAD (P)H life time in cells treated with CCCP incubated with medium than that without serum. Figure 6(c) shows the ratio of red to green fluorescence, which is an indicator for mitochondria membrane potential in cells stained with JC-1, a sensitive marker for mitochondrial membrane potential that exhibits a green to red fluorescence emission shift upon its potential-dependent accumulation in mitochondria.[55] Figures 6(d) and 6(e) show confocal microscopy images of control cells imaged in the green and red channels, while Figs. 6(f) and 6(g) show cells treated with CCCP for 1 h, both grown in medium with 3% serum. The proportional increase in green fluorescence of JC-1 after CCCP treatment indicates mitochondrial depolarization by CCCP.

The pH of the mitochondrial matrix (pH_{mit}) is higher than the cytosolic pH (pH_{cyt}). Since the addition of CCCP leads to a complete dissipation of the pH gradient over the mitochondrial inner membrane,[56] a rapid acidification of pH_{mit} is expected.[57] This has an effect on free NAD(P)H fluorescence, where the average lifetime of free NAD(P)H marginally decreases with increasing pH,[58] but is greatly affected by pH-induced structural changes to the proteins with which it interacts[59] and, therefore, the ratio of free:bound NAD(P)H. CCCP also affects the intracellular environment through the deregulation of the ion balance of the cell by the translocation of protons through membranes. Thus, the pH of the cytoplasm inside the cell equilibrates with the pH of the medium outside, which is higher than the reported intracellular pH for both pH_{mit} and pH_{cyt}.[60] Therefore, the average lifetime of both free and bound NAD(P)H is affected by changes of pH. In our system, reduction of NAD(P)H lifetime and changes in the ratio of free:bound NAD(P)H were observed only in the absence of serum (Fig. 6). We presume that serum induces undefined intracellular signaling activity that can mitigate the effects of CCCP, presumably by sustaining proton gradients. However, that conclusion remains tentative.

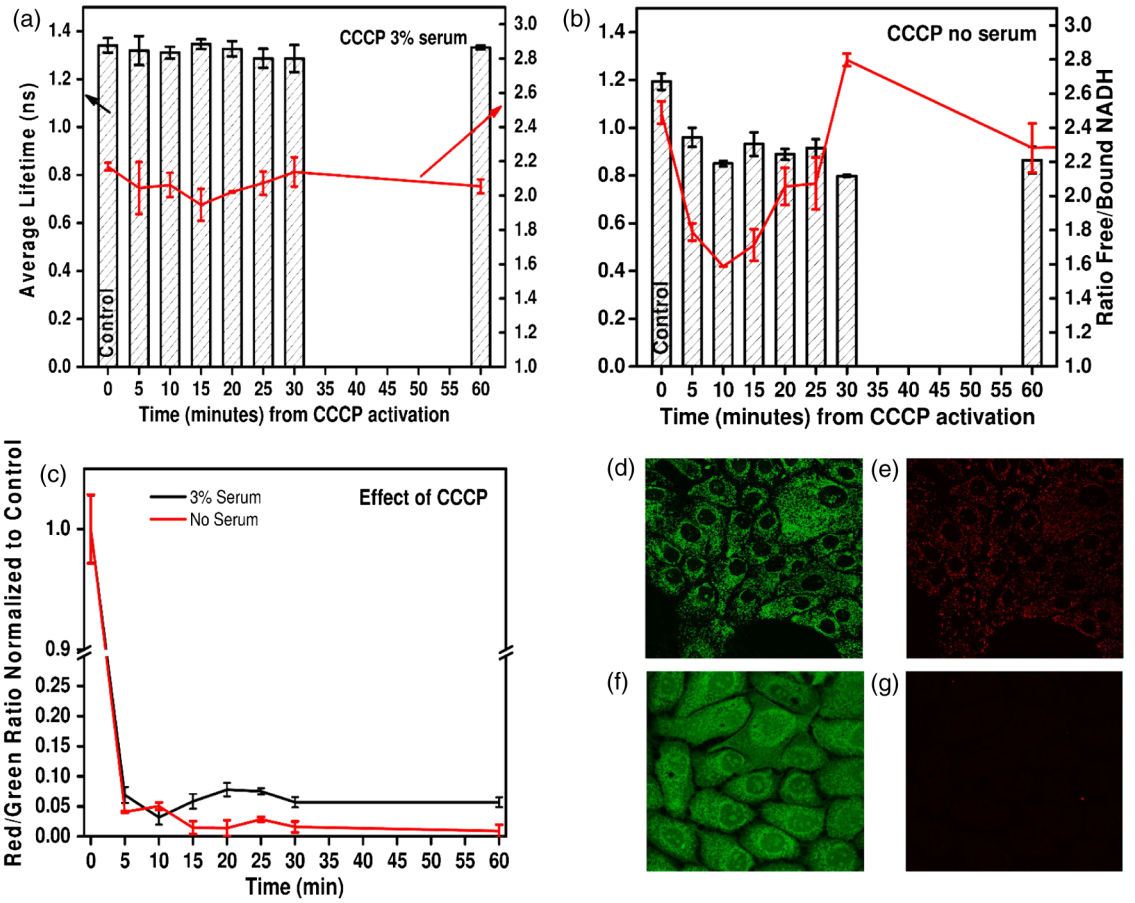

Fig. 6 Effect of carbonyl cyanide m-chlorophenylhydrazone (CCCP) inhibitor on metabolic activity of MCF10 cells measured [(a) and (b)] by lifetime measurements and (c) by staining using JC-1 membrane potential stain as a function of time from inhibitor treatment. Results shown are for the cells grown in medium with 3% serum: graph (a) and black curve in (c), and for cells grown in medium without serum: graph (b) and red curve in (c). In graph (a) and (b), average lifetime is shown as dashed bar with values corresponding to left axis and free:bound NAD(P)H ratios (ratio of contributions of short-lifetime component to long-lifetime component in measured lifetime) as red line with values corresponding to right axis. Cell images are shown for control [(d) and (e)] and for sample after 60 min from CCCP treatment [(f) and (g)], both grown in medium with 3% serum. Green images were acquired at excitation/emission of 540 nm/590 nm and red images at 570 nm/610 nm.

4 Conclusions

This study uses FLIM to evaluate and probe small changes in cellular metabolism in precancerous MCF10A cells associated with glycolysis inhibition and mitochondrial membrane dysfunction observed via changes in the average lifetime of NAD(P)H and ratios of free to bound forms of this molecule. We evaluated the effects on cellular NAD(P)H fluorescence lifetime of four different inhibitors: 2-DG, LND, OT, and 4-CMBC, which interact with different parts of the metabolic pathway, and one mitochondrial membrane uncoupler CCCP. These changes were explained on the basis of the mechanisms of inhibitors' action. The consequences for free to bound NAD(P)H ratios and average lifetimes were examined. The effect of serum on these variations was also evaluated.

Our results show that subtle features of cellular metabolism can be accurately detected by FLIM. We also established that the free-to-bound NAD(P)H ratio is a very sensitive indicator of cell metabolism and has a higher accuracy than standard biochemical methods used to assess glycolysis by measuring a lactate secretion. Multiphoton FLIM can advantageously provide functional imaging of cells where NAD(P)H fluorescence lifetime changes at the cellular level can be recorded, whereas conventional methods depend on cellular secretions, which are affected by cell count and environmental conditions. FLIM also successfully detected minute changes in free-to-bound NAD(P)H ratios in precancerous cells. We expect the outcome of this study to be a precursor for future work on the effects of these inhibitors on malignant cells, which may provide a novel way to assess the effects of inhibition of glycolysis on the differential survival of carcinogenic versus normal cells.

Acknowledgments

This work was partially supported by the Australian Research Council funded Centre of Excellence CE140100003 and conducted using instrumentation in Optical Characterization Facility at Macquarie University, link lab to AMMRF (Australian Microscopy and Microanalysis Research Facility).

References

1. J. Fang et al., "The H+-linked monocarboxylate transporter (MCT1/SLC16A1): a potential therapeutic target for high-risk neuroblastoma," *Mol. Pharmacol.* **70**(6), 2108–2115 (2006).

2. A. D. Ortega et al., "Glucose avidity of carcinomas," *Cancer Lett.* **276**(2), 125–135 (2009).
3. J. S. Fang, R. D. Gillies, and R. A. Gatenby, "Adaptation to hypoxia and acidosis in carcinogenesis and tumor progression," *Semin. Cancer Biol.* **18**(5), 330–337 (2008).
4. J. Zheng, "Energy metabolism of cancer: glycolysis versus oxidative phosphorylation (review)," *Oncol. Lett.* **4**(6), 1151–1157 (2012).
5. H. Pelicano et al., "Glycolysis inhibition for anticancer treatment," *Oncogene* **25**(34), 4633–4646 (2006).
6. E. E. Ramsay, P. J. Hogg, and P. J. Dilda, "Mitochondrial metabolism inhibitors for cancer therapy," *Pharm. Res.* **28**(11), 2731–2744 (2011).
7. R. A. Gatenby and R. J. Gillies, "Why do cancers have high aerobic glycolysis?," *Nat. Rev. Cancer* **4**(11), 891–899 (2004).
8. K. Smallbone et al., "Metabolic changes during carcinogenesis: potential impact on invasiveness," *J. Theor. Biol.* **244**(4), 703–713 (2007).
9. A. A. Heikal, "Intracellular coenzymes as natural biomarkers for metabolic activities and mitochondrial anomalies," *Biomark. Med.* **4**(2), 241–263 (2010).
10. A. F. McGettrick and L. A. O'Neill, "How metabolism generates signals during innate immunity and inflammation," *J. Biol. Chem.* **288**(32), 22893–22898 (2013).
11. A. Z. Herskovits and L. Guarente, "Sirtuin deacetylases in neurodegenerative diseases of aging," *Cell Res.* **23**(6), 746–758 (2013).
12. A. P. Gomes et al., "Declining NAD(+) induces a pseudohypoxic state disrupting nuclear-mitochondrial communication during aging," *Cell* **155**(7), 1624–1638 (2013).
13. N. D. Kirkpatrick et al., "Endogenous fluorescence spectroscopy of cell suspensions for chemopreventive drug monitoring," *Photochem. Photobiol.* **81**(1), 125–134 (2005).
14. D. Li, W. Zheng, and J. Y. Qu, "Time-resolved spectroscopic imaging reveals the fundamentals of cellular NADH fluorescence," *Opt. Lett.* **33**(20), 2365–2367 (2008).
15. M. C. Skala et al., "*In vivo* multiphoton fluorescence lifetime imaging of protein-bound and free nicotinamide adenine dinucleotide in normal and precancerous epithelia," *J. Biomed. Opt.* **12**(2), 024014 (2007).
16. W. R. Zipfel et al., "Live tissue intrinsic emission microscopy using multiphoton-excited native fluorescence and second harmonic generation," *Proc. Natl. Acad. Sci. USA* **100**(12), 7075–7080 (2003).
17. J. Vergen et al., "Metabolic imaging using two-photon excited NADH intensity and fluorescence lifetime imaging," *Microsc. Microanal.* **18**(4), 761–770 (2012).
18. J. R. Lakowicz et al., "Fluorescence lifetime imaging of free and protein-bound NADH," *Proc. Natl. Acad. Sci. USA* **89**(4), 1271–1275 (1992).
19. H. Schneckenburger et al., "Autofluorescence lifetime imaging of cultivated cells using a UV picosecond laser diode," *J. Fluoresc.* **14**(5), 649–654 (2004).
20. H. D. Vishwasrao et al., "Conformational dependence of intracellular NADH on metabolic state revealed by associated fluorescence anisotropy," *J. Biol. Chem.* **280**(26), 25119–25126 (2005).
21. M. A. Yaseen et al., "*In vivo* imaging of cerebral energy metabolism with two-photon fluorescence lifetime microscopy of NADH," *Biomed. Opt. Express* **4**(2), 307–321 (2013).
22. D. K. Bird et al., "Metabolic mapping of MCF10A human breast cells via multiphoton fluorescence lifetime imaging of the coenzyme NADH," *Cancer Res.* **65**(19), 8766–8773 (2005).
23. A. Pradhan et al., "Steady state and time-resolved fluorescence properties of metastatic and non-metastatic malignant cells from different species," *J. Photochem. Photobiol. B Biol.* **31**(3), 101–112 (1995).
24. M. Parniak and N. Kalant, "Incorporation of glucose into glycogen in primary cultures of rat hepatocytes," *Can. J. Biochem. Cell. Biol.* **63**(5), 333–340 (1985).
25. R. B. McComb and W. D. Yushok, "Metabolism of ascites tumor cells. IV. Enzymatic reactions involved in adenosinetriphosphate degradation induced by 2-deoxyglucose," *Cancer Res.* **24**, 198–205 (1964).
26. G. S. Karczmar et al., "Selective depletion of tumor ATP by 2-deoxyglucose and insulin, detected by 31P magnetic resonance spectroscopy," *Cancer Res.* **52**(1), 71–76 (1992).
27. D. Zhong et al., "2-deoxyglucose induces Akt phosphorylation via a mechanism independent of LKB1/AMP-activated protein kinase signaling activation or glycolysis inhibition," *Mol. Cancer Ther.* **7**(4), 809–817 (2008).
28. D. Lonsdale, "Thiamine," *J. Orthomol. Psychiatry* **13**(3), 197–209 (1984).
29. R. Weindruch et al., "Caloric restriction mimetics: metabolic interventions," *J. Gerontol. A, Biol. Sci. Med. Sci.* **56**(Spec No 1), 20–33 (2001).
30. B. Rais et al., "Oxythiamine and dehydroepiandrosterone induce a G1 phase cycle arrest in Ehrlich's tumor cells through inhibition of the pentose cycle," *FEBS Lett.* **456**(1), 113–118 (1999).
31. M. X. Du et al., "Identification of novel small-molecule inhibitors for human transketolase by high-throughput screening with fluorescent intensity (FLINT) assay," *J. Biomol. Screen.* **9**(5), 427–433 (2004).
32. S. H. Oh et al., "Detection of transketolase in bone marrow-derived insulin-producing cells: benfotiamine enhances insulin synthesis and glucose metabolism," *Stem Cells Dev.* **18**(1), 37–46 (2009).
33. M. Pohl, G. A. Sprenger, and M. Muller, "A new perspective on thiamine catalysis," *Current Opin. Biotechnol.* **15**(4), 335–342 (2004).
34. X. W. Chan et al., "Chemical and genetic validation of thiamine utilization as an antimalarial drug target," *Nat. Commun.* **4**, 2060 (2013).
35. C. M. Yang et al., "The *in vitro* and *in vivo* anti-metastatic efficacy of oxythiamine and the possible mechanisms of action," *Clin. Exp.Metastasis* **27**(5), 341–349 (2010).
36. K. Nath et al., "(31) P and (1) H MRS of DB-1 melanoma xenografts: lonidamine selectively decreases tumor intracellular pH and energy status and sensitizes tumors to melphalan," *NMR Biomed.* **26**(1), 98–105 (2013).
37. F. Leonetti et al., "Solid-phase synthesis and insights into structure-activity relationships of safinamide analogues as potent and selective inhibitors of type B monoamine oxidase," *J. Med. Chem.* **50**(20), 4909–4916 (2007).
38. S. Gupta et al., "FZD4 as a mediator of ERG oncogene-induced WNT signaling and epithelial-to-mesenchymal transition in human prostate cancer cells," *Cancer Res.* **70**(17), 6735–6745 (2010).
39. S. K. Gupta, "Functional study of oncogenic transcription factor ERG and its signaling in prostate cancer," PhD Thesis, Department of Pharmacology, Drug Development and Therapeutics, Institute of Biomedicine, University of Turku, Turku, Finland (2011).
40. I. Cringus-Fundeanu et al., "Synthesis and characterization of surface-grafted polyacrylamide brushes and their inhibition of microbial adhesion," *Langmuir* **23**(9), 5120–5126 (2007).
41. J. N. Anastas and R. T. Moon, "WNT signalling pathways as therapeutic targets in cancer," *Nat. Rev. Cancer* **13**(1), 11–26 (2013).
42. S. Y. Lee et al., "Wnt/snail signaling regulates cytochrome C oxidase and glucose metabolism," *Cancer Res.* **72**(14), 3607–3617 (2012).
43. E. Esen et al., "WNT-LRP5 signaling induces Warburg effect through mTORC2 activation during osteoblast differentiation," *Cell Metab.* **17**(5), 745–755 (2013).
44. A. S. Midzak et al., "ATP synthesis, mitochondrial function, and steroid biosynthesis in rodent primary and tumor Leydig cells," *Biol. Reprod.* **84**(5), 976–985 (2011).
45. P. J. Dawson et al., "MCF10AT: a model for the evolution of cancer from proliferative breast disease," *Am. J. Pathol.* **148**(1), 313–319 (1996).
46. K. M. Imbalzano et al., "Increasingly transformed MCF-10A cells have a progressively tumor-like phenotype in three-dimensional basement membrane culture," *Cancer Cell Int.* **9**(7), 1–11 (2009).
47. S. Tekkok, I. Medina, and K. Krnjevic, "Intraneuronal [Ca2+] changes induced by 2-deoxy-D-glucose in rat hippocampal slices," *J. Neurophysiol.* **81**(1), 174–183 (1999).
48. R. D. Bongard et al., "Preferential utilization of NADPH as the endogenous electron donor for NAD(P)H:quinoneoxidoreductase 1 (NQO1) in intact pulmonary arterial endothelial cells," *Free Radical Biol. Med.* **46**(1), 25–32 (2009).
49. M. P. Merker et al., "Intracellular redox status affects transplasma membrane electron transport in pulmonary arterial endothelial cells," *Am. J. Physiol. Lung Cell. Mol. Physiol.* **282**(1), L36–L43 (2002).
50. M. A. Cahill, R. Janknecht, and A. Nordheim, "Signalling pathways: jack of all cascades," *Curr. Biol.* **6**(1), 16–19 (1996).
51. R. Treisman, "The serum response element," *Trends Biochem. Sci.* **17**(10), 423–426 (1992).
52. B. K. Wright et al., "Phasor-FLIM analysis of NADH distribution and localization in the nucleus of live progenitor myoblast cells," *Microsc. Res. Tech.* **75**(12), 1717–1722 (2012).

53. L. K. Klaidman, A. C. Leung, and J. D. Adams Jr., "High-performance liquid chromatography analysis of oxidized and reduced pyridine dinucleotides in specific brain regions," *Anal. Biochem.* **228**(2), 312–317 (1995).
54. A. Floridi et al., "Enhancement of doxorubicin content by the antitumor drug lonidamine in resistant Ehrlich ascites tumor cells through modulation of energy metabolism," *Biochem. Pharmacol.* **56**(7), 841–849 (1998).
55. S. T. Smiley et al., "Intracellular heterogeneity in mitochondrial membrane potentials revealed by a J-aggregate-forming lipophilic cation JC-1," *Proc. Natl. Acad. Sci. USA* **88**(9), 3671–3675 (1991).
56. R. Orij et al., "*In vivo* measurement of cytosolic and mitochondrial pH using a pH-sensitive GFP derivative in Saccharomyces cerevisiae reveals a relation between intracellular pH and growth," *Microbiology* **155**(1), 268–278 (2009).
57. A. Takahashi et al., "Measurement of mitochondrial pH *in situ*," *BioTechniques* **30**(4), 804–808, 810, 812 passim (2001).
58. S. Ogikubo et al., "Intracellular pH sensing using autofluorescence lifetime microscopy," *J. Phys. Chem. B* **115**(34), 10385–10390 (2011).
59. N. Hano et al., "Effect of pH on the steady state kinetics of bovine heart NADH: coenzyme Q oxidoreductase," *J. Bioenerg. Biomembr.* **35**(5), 419–425 (2003).
60. J. Haveman, "The pH of the cytoplasm as an important factor in the survival of *in vitro* cultured malignant cells after hyperthermia. Effects of carbonylcyanide 3-chlorophenylhydrazone," *Eur. J. Cancer* **15**(10), 1281–1288 (1979).

Krystyna Drozdowicz-Tomsia is a research fellow with 30 years of research experience in diverse range of areas and a member of MQ BioFocus Research Centre. Her current research focuses on ultrasensitive detection of trace analytes by using biophotonics, plasmonics, and nanotechnology. She has expertise in various spectroscopy techniques, immunochemistry, advanced image acquisition and processing, including methods based on autofluorescence using fluorescence lifetime imaging (FLIM) and hyperspectral image analysis applied to biomedical sensing and cancer research.

Ayad G. Anwer is a research fellow and a member of MQ BioFocus Research Centre at Macquarie University. He was employed as an associate professor at the University of Baghdad before receiving a prestigious Endeavour Australian Fellowship at Macquarie University. His research focuses on laser applications in biology and biophotonics, correlative confocal and electron microscopy, biological specimen preparation, biostimulation, and advanced optical characterization methods based on autofluorescence, including FLIM and hyperspectral image analysis.

Michael A. Cahill has 30 years of international research experience in both academic and industrial settings. As scientific cofounder and chief research officer of ProteoSys AG, Mainz, Germany, from 2000 to 2007, he was responsible for the development of the proprietary ProteoTope proteomics technology platform and its application to breast and prostate cancer discovery projects. He currently lectures in biochemistry and cell biology, and researches cancer cell biology.

Kaiser N. Madlum received a PhD degree in biology from the Institute of Laser for Post Graduate Studies, Baghdad University in 2013. He was an assistant lecturer (2006 to 2010) in the Department of Biology, College of Science, Babylon University, Iraq, before moving to the College of Medicine in the same university. He is currently a lecturer in the Department of Histology and Anatomy at Babylon University.

Amel M. Maki currently works as an assistant professor in the Biomedical Department, Institute of Laser for Postgraduate Studies, University of Baghdad, Iraq. She received a PhD degree in zoology from University College Dublin, Ireland, in 1986, where she also became a postdoctoral researcher in the School of Biology and Environmental Science during 2007 to 2009. Her research concentrates on effects of laser irradiation and bio-stimulation on cells as well as analysis of various bio-indicators in diverse ecosystems.

Mark S. Baker is an internationally recognized cancer researcher and president-elect of the Human Proteome Organization. His most recent work has focused on membrane proteome and mechanisms by which ovarian, colon, breast, and prostate cancer develop. As a former director of Biomarker Discovery at LumiCyte Mark, he has senior management experience in academic, industrial, and clinical cancer discovery settings, translating ideas into commercial reality, especially in the area of platform development.

Ewa M. Goldys is the deputy director of the Australian Research Council Centre of Excellence in Nanoscale Biophotonics and director of MQ BioFocus Research Centre at Macquarie University. Her research focuses on ultrasensitive detection of trace analytes by using biophotonics and nanotechnology. She is a fellow of the Optical Society of America for research leadership in optical characterization and biomedical sensing, which has promoted widespread interdisciplinary awareness of light in life sciences.